KSCE Journal of Civil Engineering (2020) 24(5):1531-1544
DOI 10.1007/s12205-020-0816-5

pISSN 1226-7988, eISSN 1976-3808
www.springer.com/12205

Structural Engineering

Vibration Analysis of EMS-Type Maglev Vehicles Traveling over a Long-Span Bridge with Double Lines

Wei Liu[a] **and Wenhua Guo**[a]

[a]*Dept. of Civil Engineering, Central South University, Changsha 410075, China*

ARTICLE HISTORY

Received 8 May 2019
Accepted 9 February 2020
Published Online 25 March 2020

KEYWORDS

EMS-type maglev vehicles
Long-span bridge
Vehicle-bridge interaction
Principle of virtual work
Separated iterative approach

ABSTRACT

This paper establishes a detailed three-dimensional (3D) model to study the spatial vibration characteristics of two middle-low speed vehicles traveling along a long-span bridge with double lines. Here, two state-space equations for the left- and right-hand maglev vehicles are derived, considering the equations of motion of vehicles, governing equations of currents, linear feedback controls and state observers. By employing the conventional finite element method, the equation of motion for the variable cross-section continuous girder bridge with three spans is simulated. To solve these three coupled equations, this study adopted a new separated iterative approach based on the precise integration method and the Newmark-β method. The total virtual work conducted by the inertial loads, damping loads, elastic loads and fluctuating electromagnetic loads are calculated to conveniently assemble the global mass matrix, damping matrix, stiffness matrix and coefficient matrices of fluctuating electromagnetic forces in the maglev vehicles. The numerical studies indicate that the vertical interactions play dominant roles in the 3D maglev vehicles-bridge system, and the passing maglev vehicles on the bridge have little influence on the lateral motions of the vehicle on the other line due to the adequate lateral stiffness of the bridge.

1. Introduction

The application of magnetically levitated (maglev) technologies in transport has developed rapidly since the 1970s (Glatzel et al., 1980). The two effective suspension technologies in practical maglev vehicle systems are electrodynamic suspension (EDS) and electromagnetic suspension (EMS) (Kaloust et al., 2004). The EDS system suspends a vehicle above its guide-rail based on repulsive forces between superconducting magnets on the vehicle and the normal coils on the guideway, while the EMS system employs the attractive forces between the conventional electromagnets on the vehicles and the ferromagnetic rails to levitate the vehicle towards steel tracks. The other major difference is that the EMS system is unstable without controls and the EDS system can maintain self-stabilization at high speeds (Park et al., 2001). In the past two decades, the EMS-type train has achieved commercial application in Japan, Korea and China (Suzuki et al., 1984; Kwon et al., 2008; Zhang and Huang, 2019). In this paper, the vibration analysis of the EMS-type maglev vehicles traveling over the long-span space continuous girder bridge is based on the Changsha Maglev Express (CME) with middle-low speed in China.

The dynamic behavior of maglev vehicles has important consequences for the safety, ride quality, guideway design and system cost. To design a proper guideway that proves the maglev vehicle with an acceptable ride quality, the dynamic characteristics of the maglev vehicle-guideway system must be understood. Therefore, many investigators have conducted extensive investigations for the dynamic interaction of the EMS-type maglev vehicle running on the flexible guideway. Popp and Schiehlen (1975) previously established a simplified maglev vehicle-guideway model in which the vehicle is modelled using two lumped masses connected by a spring-damper system. Cai et al. (1992; 1994) provided a detailed description of vertical motions for 9-degrees-of-freedom (9-DOF) maglev vehicle moving along guideway. These authors also reviewed the various aspects of the dynamic characteristics, experiments and analysis, and design guidelines for the simple maglev-guideway systems (Cai and Chen, 1997). Zheng et al. (2005) studied the vertical dynamic stability of a simplified model with 2-DOF using the Lyapunov

CORRESPONDENCE Wenhua Guo whguo@126.com Dept. of Civil Engineering, Central South University, Changsha 410075, China

exponent. To evaluate the ride quality of maglev vehicle moving on different types of guideways, Zhao and Zhai (2002) developed a 10-DOF model of maglev vehicle and the discrete fast Fourier transform is employed for the random response results. Then, more complicated maglev vehicle-guideway models have been developed based on the numerical techniques and control laws. Yau (2009; 2010a; 2010b; 2010c) carried out a systematic study in a simple maglev vehicle-guideway system with vibration control, resonance phenomena and environmental excitations. Shi et al. (2007) established a 3D dynamic model of the high-speed maglev vehicle and guideway interaction. Based on the urban transit maglev (UTM) in Korea, Min et al. (2017) presented a detailed 3D model with 25-DOF to study the dynamic interaction effects of guideways and vehicles, including vertically and laterally resonant vibrations. Treating the 3D vehicle model as the rigid bodies with 55-DOF and considering a real continuous girder bridge, Liu and Guo (2019) conducted the linear random vibration of maglev vehicle-bridge system. However, there is little research considering the motions of EMS-type maglev vehicles moving over a long-span bridge with double lines.

The purpose of this study is to develop a detailed 3D model of multicar maglev vehicles traveling over a long-span bridge with double lines. Two derived state-space equations of left- and right-hand maglev vehicles consider the equations of motion of vehicles, governing equations of currents, linear feedback controls and state observers. These two state-space equations of the vehicles and the equation of motion of the bridge are coupled via electromagnetic forces, and they are solved by a new separated iterative approach based on the precise integration method and the Newmark-β method. The virtual work performed by all inertial forces, damping forces, elastic forces and fluctuating electromagnetic forces are calculated to conveniently assemble the global mass matrix, damping matrix, stiffness matrix and coefficient matrices of fluctuating electromagnetic forces in the maglev vehicles. Some objective facts verify the correctness of the proposed 3D model that when two sets of maglev vehicles move on the bridge with smooth guideway at same traveling speeds, the cabin vertical displacements for left- and right-hand maglev vehicles are exactly the same, and their lateral displacements ought to be completely opposite. The effects of guideway irregularities on the maglev vehicles-bridge system are considered in this model. Additionally, the numerical simulations investigate the effects of the traveling speeds and the number of cars on the maglev vehicles running on the long-span continuous girder bridge.

2. Model of Maglev Vehicles

As shown in Fig. 1, a full 3D maglev vehicle is simulated using one cabin body supported by secondary suspensions connected with ten levitation bogies, in which the secondary suspensions are simplified by adopting longitudinal, vertical and horizontal spring-dashpot systems. Interactions between left- and right-hand anti-roll beams rigidly connected with bogies are modelled using 20 groups of vertical and lateral spring-dashpot systems. Each bogie has four suspension magnets, and there exist 40 suspension magnets in a car. It should be noted that fixed sliding tables and lateral sliding tables are used to link the cabin to the secondary suspensions. Major difference in these two tables is that the fixed sliding table can fasten two connectors in three directions of space, while the lateral sliding stable merely fixes two connectors in the vertical direction. Table 1 shows the corresponding parameters of the maglev system.

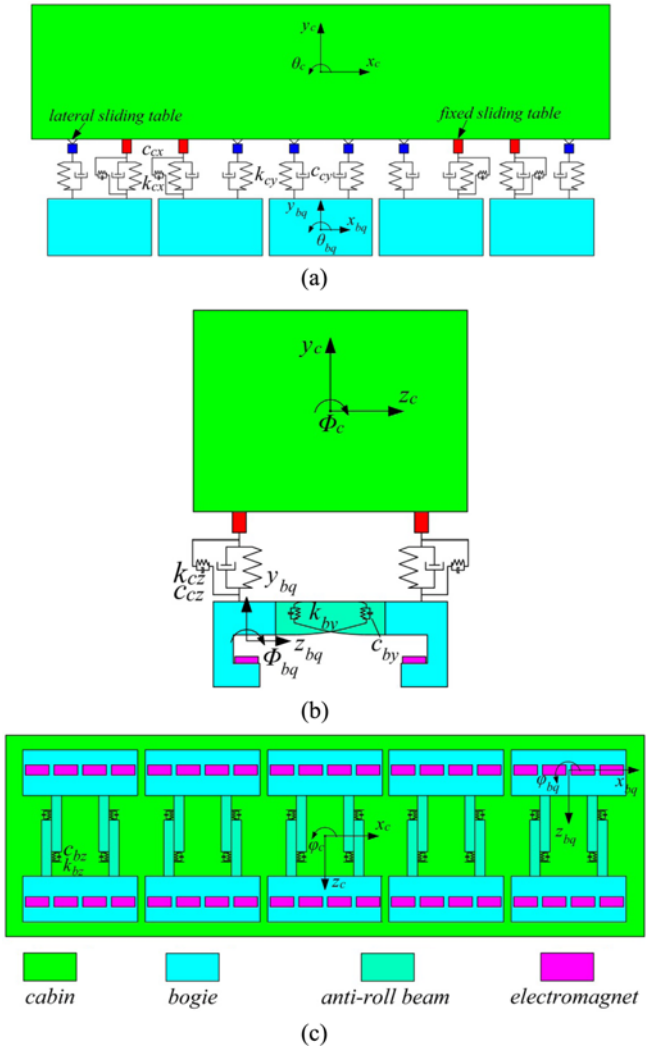

Fig. 1. Maglev Vehicle Model: (a) Side View, (b) Front View, (c) Plane View

2.1 Electromagnetic Force

The electromagnetic forces couple maglev vehicles and the bridge. Unlike the traditional ground transportation in which the interactions come from the contact forces, the noncontact maglev vehicles-guideway system is still subjected to the effects of the electromagnetic forces. The electromagnetic force is usually expressed by (Kong et al., 2011):

$$F = \frac{\mu_0 A_0 N_0^{\ 2}}{4}\left(\frac{i}{h}\right)^2 \tag{1}$$

where μ_0 is the permeability factor, A_0 is the pole face area, N_0 is the number of turns coil, h is the vertical air gap between the magnet and the guideway, and i is the control current. Considering that the electromagnetic force fluctuates slightly up and down at the balance point, the nonlinear electromagnetic force can be translated into the linear electromagnetic force using a Taylor series expansion at the balance point and the following expressions have ignored the effect of high order derivative.

$$F = \frac{\mu_0 A_0 N_0^2 i_0^2}{4h_0^2} + \frac{\mu_0 A_0 N_0^2 i_0}{2h_0^2}\Delta i - \frac{\mu_0 A_0 N_0^2 i_0^2}{2h_0^3}\Delta h \tag{2}$$

$$G_0 = \frac{\mu_0 A_0 N_0^2 i_0^2}{4h_0^2} = \left(\frac{m_c}{\rho_1} + \frac{m_b}{\rho_2}\right)\mathrm{g} \tag{3}$$

$$\Delta F = \frac{\mu_0 A_0 N_0^2 i_0}{2h_0^2}\Delta i - \frac{\mu_0 A_0 N_0^2 i_0^2}{2h_0^3}\Delta h = k_i \Delta i - k_h \Delta h \tag{4}$$

where i_0 and h_0 are the nominal current and air gap, respectively, Δi and Δh are the fluctuating current and air gap, respectively, k_i and k_h are the equivalent stiffness, g is the gravitational acceleration, and m_c and m_b are the lump mass of the cabin and bogie, respectively. Note that the magnetic force G_0 at the static equilibrium point is equivalent to the gravity at corresponding position produced by the cabin and bogies. Here, due to symmetric distribution of configuration of the maglev vehicle, $\rho_1 = 40$ is the number of electromagnetic forces in one vehicle and $\rho_2 = 4$ is the number of electromagnetic forces in one bogie.

Each two adjacent electromagnetic forces share a control current, and a bogie has two control fluctuating currents. The total number of the control currents is 20 in the maglev vehicle with one car. The first-order derivative of the fluctuating current Δi in Eq. (4) can be described by (Kim et al., 2015):

$$\Delta \dot{i}_p = \frac{i_0}{h_0}\Delta \dot{h}_p - \frac{R_0}{L_0}\Delta i_p + \frac{1}{L_0}\Delta U_p \tag{5}$$

$$L_0 = \frac{\mu_0 N_0^2 A_0}{2h_0} \tag{6}$$

where subscript p = 1, 2, 3, …, 20, ΔU_p is the pth fluctuating voltage, L_0 is the inductance of the magnet winding, and Δh_p is the first-order derivative of the mean value of two adjacent air gaps in the vertical direction.

As the laterally independent control system does not exist in the middle-low speed EMS-type maglev vehicle, the simplified lateral electromagnetic force ΔF_e can be given as (Min et al., 2017):

$$\Delta F_e = -k_e \Delta z_e \tag{7}$$

where $k_e = 2G_0/\pi d_0$. ΔF_e is the lateral guide force, k_e is the equivalent stiffness, Δz_e is the lateral air gap between the magnet and the guideway, and d_0 is the width of the magnet on the bogie.

2.2 Model of Maglev Vehicle with One Car

2.2.1 Equation of Motion

In the maglev vehicle with one car, the cabin and bogies are considered as rigid bodies. Each rigid body considers 5-DOF, namely, lateral and vertical displacements as well as rolling, pitching and yawing rotations. The 11 rigid bodies in the car have total 55-DOF. Hence, the displacement vector can be described by:

$$\begin{aligned}\mathbf{Y}_m = [&y_c, z_c, \Phi_c, \varphi_c, \theta_c, y_{b1}, z_{b1}, \Phi_{b1}, \varphi_{b1}, \theta_{b1}, \cdots,\\ &y_{bq}, z_{bq}, \Phi_{bq}, \varphi_{bq}, \theta_{bq}]^T\end{aligned} \tag{8}$$

where y, z, Φ, φ and θ represent the vertical and lateral displacements, as well as rolling rotation, pitching and rotations, respectively, the subscripts c and b denote the cabin and bogie, respectively, the subscript q (q = 1, 2, 3, …, 10) is the qth bogie. For instance, Φ_{b4} is the rotation by the x-axis at the 4th bogie. One bogie in the vertical direction is supported by four electromagnetic forces because it is reasonable that uniformly distributed forces between the electromagnets and ferromagnetic rails are assumed to be concentrated force (Cai et al., 1992). There are 40 electromagnetic forces and guide forces in one car. Accordingly, the required vertical guideway displacements in the vertical air gaps can be determined as following vector form:

$$\mathbf{U} = [u_1, u_2, u_3, \cdots, u_r]^T \tag{9}$$

The lateral guideway displacement vector related to lateral air gaps is:

$$\mathbf{V} = [v_1, v_2, v_3, \cdots, v_r]^T \tag{10}$$

and the fluctuating current vector in the fluctuating electromagnetic forces is:

$$\Delta \mathbf{I}_m = [\Delta i_1, \Delta i_2, \Delta i_3, \cdots, \Delta i_{p-1}, \Delta i_p]^T \tag{11}$$

where u_r and v_r are, respectively, the rth vertical and lateral guideway displacements and subscript r has the maximum value of 40, Δi_p is the pth control current and subscript p has the maximum value of 20. Both vertical and lateral guideway displacements contain two parts of bridge displacements and guideway irregularities.

In general, the equation of motion for the maglev vehicle is:

$$\mathbf{M}_m \ddot{\mathbf{Y}}_m + \mathbf{C}_m \dot{\mathbf{Y}}_m + \mathbf{K}_m \mathbf{Y}_m = \Delta \mathbf{F}_m \tag{12}$$

in which $\mathbf{M}_m$, $\mathbf{C}_m$ and $\mathbf{K}_m$ are the mass, damping and stiffness matrices of the car, respectively, and $\Delta \mathbf{F}_m$ is the force vector. As the maglev vehicles-bridge model will be solved by the separated iterative method, vehicles are treated as an independent system, and the influences of guideway displacements on the car should be considered as external inputs. According to the calculations of vertically and laterally fluctuating electromagnetic forces in Eqs. (4) and (7), one can know that the matrix-vector form of the force vector in Eq. (12) can be written as:

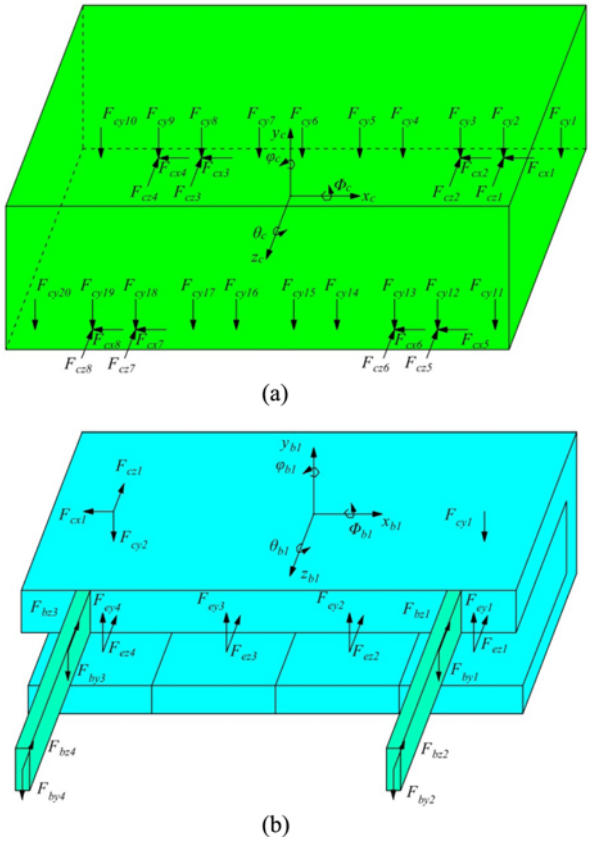

Fig. 2. Free Body Diagrams of: (a) The Cabin, (b) The First Bogie

$$\Delta\mathbf{F}_m = \mathbf{A}_m\mathbf{Y}_m + \mathbf{B}_m\Delta\mathbf{I}_m + \mathbf{E}_m\mathbf{U} + \mathbf{Q}_m\mathbf{V} \tag{13}$$

where $\mathbf{A}_m$, $\mathbf{B}_m$, $\mathbf{E}_m$ and $\mathbf{Q}_m$ are the coefficient matrices.

Displayed in Fig. 2 are the free body diagrams of the cabin and the first bogie, where F_{cxu}, F_{cyg} and F_{czu} ($u = 1, 2, 3, \ldots, 8$ and $g = 1, 2, 3, \ldots, 20$) are the longitudinal, vertical and lateral forces, including the damping and spring forces supporting the cabin, F_{byf} and F_{bzf} ($f = 1, 2, 3, \ldots, 20$) are the vertical and lateral forces containing damping and spring forces between the left- and right-hand bogies, F_{byr} and F_{bzr} are the vertical and lateral electromagnetic forces, respectively. According to the principle of virtual work, the virtual work of the vehicle performed by all inertial forces, damping forces, elastic forces, electromagnetic forces and guide forces can be described as following expression:

$$\delta W_m = \delta W_a + \delta W_{cx} + \delta W_{cy} + \delta W_{cz} + \delta W_{by} + \delta W_{bz} + \delta W_{ey} + \delta W_{ez} \tag{14}$$

where δW_m denotes the total virtual work of all forces in one car, δW_a represents the total virtual work of all inertia forces, δW_{cx}, δW_{cy} and δW_{cz} are the total virtual work done by secondary spring-damper systems in the longitudinal, vertical and lateral directions, respectively, δW_{by} and δW_{bz} are the total virtual work done by spring-damper systems connecting bogies for vertical and lateral directions, respectively, δW_{ey} and δW_{ez} are the total virtual work done by vertical and lateral electromagnetic forces, respectively. Furthermore, these virtual works can be rewritten as the following expressions.

$$\delta W_a = \delta y_c m_c \ddot{y}_c^2 + \delta z_c m_c \ddot{z}_c^2 + \delta\Phi_c J_{cx}\ddot{\Phi}_c^2 + \delta\varphi_c J_{cy}\ddot{\varphi}_c^2 + \delta\theta_c J_{cz}\ddot{\theta}_c^2 + \sum_{q=1}^{10}(\delta y_{bq} m_b \ddot{y}_{bq}^2 + \delta z_{bq} m_b \ddot{z}_{bq}^2 + \delta\Phi_{bq} J_{bx}\ddot{\Phi}_{bq}^2 + \delta\varphi_{bq} J_{by}\ddot{\varphi}_{bq}^2 + \delta\theta_{bq} J_{bz}\ddot{\theta}_{bq}^2) \tag{15}$$

$$\delta W_{cx} = \sum_u^8 \delta W_{cxu} = \sum_u^8 F_{cxu}\delta\Delta_{cxu} = \sum_u^8 (k_{cx}\delta\Delta_{cxu}\Delta_{cxu} + c_{cx}\delta\Delta_{cxu}\dot{\Delta}_{cxu}) \tag{16}$$

$$\delta W_{cy} = \sum_g^{20} \delta W_{cyg} = \sum_g^{20} F_{cyg}\delta\Delta_{cyg} = \sum_g^{20} (k_{cy}\delta\Delta_{cyg}\Delta_{cyg} + c_{cy}\delta\Delta_{cyg}\dot{\Delta}_{cyg}) \tag{17}$$

$$\delta W_{cz} = \sum_u^8 \delta W_{czu} = \sum_u^8 F_{czu}\delta\Delta_{czu} = \sum_u^8 (k_{cz}\delta\Delta_{czu}\Delta_{czu} + c_{cz}\delta\Delta_{czu}\dot{\Delta}_{czu}) \tag{18}$$

$$\delta W_{by} = \sum_f^{20} \delta W_{byf} = \sum_f^{20} F_{byf}\delta\Delta_{byf} = \sum_f^{20} (k_{by}\delta\Delta_{byf}\Delta_{byf} + c_{by}\delta\Delta_{byf}\dot{\Delta}_{byf}) \tag{19}$$

$$\delta W_{bz} = \sum_f^{20} \delta W_{bzf} = \sum_f^{20} F_{bzf}\delta\Delta_{bzf} = \sum_f^{20} (k_{bz}\delta\Delta_{bzf}\Delta_{bzf} + c_{bz}\delta\Delta_{bzf}\dot{\Delta}_{bzf}) \tag{20}$$

$$\delta W_{ey} = \sum_r^{40} \delta W_{eyr} = \sum_{r=1}^{40} F_{eyr}\delta\Delta h_{eyr} = \sum_{r=2p}^{40} \delta\Delta h_{eyr}(k_i\Delta i_p - k_h\Delta h_{eyr}) + \sum_{r=2p-1}^{40} \delta\Delta h_{eyr}(k_i\Delta i_p - k_h\Delta h_{eyr}) \tag{21}$$

$$\delta W_{ez} = \sum_{r=1}^{40} \delta W_{ezr} = \sum_{r=1}^{40} -F_{ezr}\delta\Delta z_{ezr} = \sum_{r=1}^{40} -k_{ez}\delta\Delta z_{ezr}\Delta z_{ezr} \tag{22}$$

where Δ_{cxu}, Δ_{cyg} and Δ_{czu} are the relative displacements in the longitudinal, vertical and lateral directions for the secondary suspensions, respectively; Δ_{byf} and Δ_{bzf} are the relative displacements in the vertical and lateral directions between bogies, respectively; Δh_{eyr} and Δz_{ezr} are the vertical and lateral air gaps, respectively; k_{cx} and c_{cx}, k_{cy} and c_{cy}, and k_{cz} and c_{cz} are the stiffness and damping coefficients of the longitudinal, vertical and lateral secondary spring-dampers, respectively; k_{by} and c_{by}, and k_{bz} and c_{bz} are the stiffness and damping coefficients of the vertical and lateral spring-dampers connecting bogies, respectively; J_{cx}, J_{cy} and J_{cz} are the rolling, pitching and yawing moments of inertia of the cabin body, respectively; and J_{bx}, J_{by} and J_{bz} are the rolling, pitching and yawing moments of inertia of the bogie, respectively.

Further calculating Eqs. (15) – (22) will again produce many terms and all terms can be divided into the following seven categories: $\delta y_\gamma A_K y_\eta$, $\delta y_\gamma A_C \dot{y}_\eta$, $\delta y_\gamma A_M \ddot{y}_\eta$, $\delta y_\gamma A_A y_\eta$, $\delta y_\gamma A_B i_\vartheta$, $\delta y_\gamma A_E u_\chi$ and $\delta y_\gamma A_Q v_\chi$, where $1 \le \gamma \le 55$, $1 \le \eta \le 55$, $1 \le \vartheta \le 20$ and $1 \le \chi \le 40$. y_γ and δy_η express the γth and ηth elements in the displacement vector $\mathbf{Y}_m$ and the virtual displacement vector $\delta\mathbf{Y}_m$, respectively. i_ϑ is the ϑth element in the vector $\Delta\mathbf{I}_m$. u_χ and v_χ are the χth elements in the vectors $\mathbf{U}$ and $\mathbf{V}$, respectively. A_K, A_C, A_M, A_A, A_B, A_E and A_Q are the coefficients, and all of these coefficients can be automatically added to the corresponding position of the matrices $\mathbf{K}_m$, $\mathbf{C}_m$, $\mathbf{M}_m$, $\mathbf{A}_m$, $\mathbf{B}_m$, $\mathbf{E}_m$ and $\mathbf{Q}_m$ in the computer program, respectively. After all these terms are assembled, the stiffness matrix, damping matrix, mass matrix and the coefficient matrices of electromagnetic force for the car are built. For instance, the coefficient A_A can be automatically added to the coefficient matrix $\mathbf{A}_m$ at the γth row and the ηth column. When subscript $r = 1$, the virtual work of the first lateral guide force can be written as:

$$
\begin{aligned}
-k_{ez}\delta\Delta z_{ez1}\Delta z_{ez1} &= -k_{ez}\delta(z_{b1}+H_{ey1}\Phi_{b1}-H_{ex1}\varphi_{b1}-v_1)\\
&\quad (z_{b1}+H_{ey1}\Phi_{b1}-H_{ex1}\varphi_{b1}-v_1)\\
&= -\delta z_{b1}k_{ez}z_{b1}-\delta\Phi_{b1}H_{ey1}k_{ez}z_{b1}+\delta\varphi_{b1}H_{ex1}k_{ez}z_{b1}\\
&\quad -\delta z_{b1}H_{ey1}k_{ez}\Phi_{b1}-\delta\Phi_{b1}H_{ey1}k_{ez}H_{ey1}\Phi_{b1}+\delta\varphi_{b1}H_{ex1}k_{ez}H_{ey1}\Phi_{b1}\\
&\quad +\delta z_{b1}k_{ez}H_{ex1}\varphi_{b1}+\delta\Phi_{b11}H_{ey1}k_{ez}H_{ex1}\varphi_{b1}-\delta\varphi_{b1}H_{ex1}k_{ez}H_{ex1}\varphi_{b1}\\
&\quad +\delta z_{b1}k_{ez}v_1+\delta\Phi_{b1}H_{ey1}k_{ez}v_1-\delta\varphi_{b1}H_{ex1}k_{ez}v_1
\end{aligned}
\tag{23}
$$

where H_{ex1} and H_{ey1} are the longitudinal and vertical coordinates of the first lateral guide force based on the local coordinate system of the first bogie on the left-hand side of the car. Obviously, each item in the Eq. (23) is one of two categories of $\delta y_\gamma A_A y_\eta$ and $\delta y_\gamma A_Q v_\chi$. All of these two kinds of coefficients can be automatically added to corresponding positions of the matrices $\mathbf{A}_m$ and $\mathbf{Q}_m$ in the computer program.

2.2.2 Governing Equation of Fluctuating Current

Stable fluctuating voltage in the EMS-type maglev vehicle is a key factor to keep the vehicle travel safely on the guideway. Without appropriate control voltage, the vehicle cannot produce the required fluctuating current. To produce the control voltage, we introduce the linear negative feedback control, which is expressed as follows (Shi et al., 2007 and Sinha et al., 1991):

$$
\Delta U_p = -k_a\ddot{y}_p - k_v\Delta\dot{h}_p - k_d\Delta h_p \tag{24}
$$

where Δh_p is the pth mean value of two adjacent air gaps in the vertical direction, $\ddot{y}_p$ is the corresponding acceleration related to the pth control voltage, and k_d, k_v and k_a are the coefficients of the feedback control.

The sensors on the bogies are able to measure the relative displacements and accelerations of the vertical air gaps, but it is difficult to measure the relative velocities. However, the relative velocity can be estimated by using the state observer. For the purpose of convenience in calculation, the relative displacement Δh_p in Eq. (24) is also set as an estimated variable. Hence, based on Eqs. (5) and (24), the matrix-vector form of the governing equation of the fluctuating control current can be given as:

$$
\Delta\dot{\mathbf{I}}_m = \mathbf{D}_m\ddot{\mathbf{Y}}_m + \mathbf{G}_m\Delta\mathbf{I}_m + \mathbf{J}_m\Delta\dot{\hat{\mathbf{H}}}_m + \mathbf{O}_m\Delta\hat{\mathbf{H}}_m \tag{25}
$$

where $\Delta\hat{\mathbf{H}}_m$ is the vector of the estimated variable for the vertical air gap, $\mathbf{D}_m$, $\mathbf{G}_m$, $\mathbf{J}_m$ and $\mathbf{O}_m$ are the coefficient matrices, in which all elements can be automatically assembled row by row in the computer program. The following will take an example of assembling the first rows. Substituting Eq. (24) into Eq. (5), the first-order derivative of the control current is described as follows:

$$
\begin{aligned}
\Delta\dot{i}_1 &= -\frac{k_a}{L_0}\ddot{y}_1 - \frac{R_0}{L_0}\Delta i_1 + \left(\frac{i_0}{h_0}-\frac{k_v}{L_0}\right)\Delta\dot{\hat{h}}_1 - \frac{k_d}{L_0}\Delta\hat{h}_1\\
&= -\frac{k_a}{2L_0}(\ddot{y}_{b1} - H_{ez1}\ddot{\Phi}_{b1} + H_{ex1}\ddot{\theta}_{b1} + \ddot{y}_{b1} - H_{ez2}\ddot{\Phi}_{b1} + H_{ex2}\ddot{\theta}_{b1}) - \frac{R_0}{L_0}\Delta i_1\\
&\quad +\frac{1}{2}\left(\frac{i_0}{h_0}-\frac{k_v}{L_0}\right)(\Delta\dot{\hat{h}}_{ey1}+\Delta\dot{\hat{h}}_{ey2}) - \frac{k_d}{2L_0}(\Delta\hat{h}_{ey1}+\Delta\hat{h}_{ey2})\\
&= -\frac{k_a}{L_0}\ddot{y}_{b1} + \frac{k_aH_{ez1}}{2L_0}\ddot{\Phi}_{b1} - \frac{k_aH_{ex1}}{2L_0}\ddot{\theta}_{b1} + \frac{k_aH_{ez2}}{2L_0}\ddot{\Phi}_{b1} - \frac{k_aH_{ex2}}{2L_0}\ddot{\theta}_{b1} - \frac{R_0}{L_0}\Delta i_1\\
&\quad +\frac{1}{2}\left(\frac{i_0}{h_0}-\frac{k_v}{L_0}\right)\Delta\dot{\hat{h}}_{ey1} + \frac{1}{2}\left(\frac{i_0}{h_0}-\frac{k_v}{L_0}\right)\Delta\dot{\hat{h}}_{ey2} - \frac{k_d}{2L_0}\Delta\hat{h}_{ey1} - \frac{k_d}{2L_0}\Delta\hat{h}_{ey2}
\end{aligned}
\tag{26}
$$

where H_{ez1} is the lateral coordinate of the first electromagnetic force based on the local coordinate system of the first bogie on the left-hand of the cabin, H_{ex2} and H_{ez2} are the longitudinal and lateral coordinates, respectively, of the second electromagnetic force based on the local coordinate system of the first bogie, $\Delta\hat{h}_{ey1}$ and $\Delta\dot{\hat{h}}_{ey1}$ are the estimated vertical air gap and its first-order derivative related to the first electromagnetic force, $\Delta\hat{h}_{ey2}$ and $\Delta\dot{\hat{h}}_{ey2}$ are the estimated vertical air gaps and its first-order derivative related to the second electromagnetic force. Each term in Eq. (26) should be one of following four categories: $A_D\ddot{y}_\eta$, $A_G\Delta i_\vartheta$, $A_J\Delta\dot{\hat{h}}_\chi$ and $A_O\Delta\hat{h}_\chi$. Δi_ϑ represents the ϑth element of $\Delta\mathbf{I}_m$, and $\Delta\hat{h}_\chi$ and $\Delta\dot{\hat{h}}_\chi$ represent the χth elements of $\Delta\hat{\mathbf{H}}_m$ and $\Delta\dot{\hat{\mathbf{H}}}_m$, respectively. Finally, these four types of coefficients A_D, A_G, A_J and A_O are added to corresponding positions in the first rows of the $\mathbf{D}_m$, $\mathbf{G}_m$, $\mathbf{J}_m$, and $\mathbf{O}_m$, respectively. After the remaining 19 rows of these coefficient matrices are assembled in this way, the work of forming the governing equation of fluctuating current is finished entirely.

2.2.3 State Observer

In the maglev vehicle-bridge system, to estimate un-measurable state variables, a state observer is required to design. The state variables to be estimated are $\Delta\mathbf{H}_m$ and $\Delta\dot{\mathbf{H}}_m$. As vertical air gaps and their second derivatives can be measured by using sensors on the bogies, a state-space equation based on these measured variables is formulated as follows:

$$
\begin{Bmatrix}\Delta\dot{\mathbf{H}}_m\\ \Delta\ddot{\mathbf{H}}_m\end{Bmatrix} = \begin{bmatrix}\mathbf{0} & \mathbf{1}\\ \mathbf{0} & \mathbf{0}\end{bmatrix}\begin{Bmatrix}\Delta\mathbf{H}_m\\ \Delta\dot{\mathbf{H}}_m\end{Bmatrix} + \begin{Bmatrix}\mathbf{0}\\ \Delta\ddot{\mathbf{H}}_m\end{Bmatrix} \tag{27}
$$

$$
\Delta\mathbf{H}_m = [\mathbf{1}\quad\mathbf{0}]\begin{Bmatrix}\Delta\mathbf{H}_m\\ \Delta\dot{\mathbf{H}}_m\end{Bmatrix} \tag{28}
$$

where $\mathbf{0}$ and $\mathbf{1}$ are the zero matrix and unit matrix. As a result, the state-space equation of the corresponding state observer is constructed as:

$$
\begin{Bmatrix}\Delta\dot{\hat{\mathbf{H}}}_m\\ \Delta\ddot{\hat{\mathbf{H}}}_m\end{Bmatrix} = \begin{bmatrix}\mathbf{0} & \mathbf{1}\\ \mathbf{0} & \mathbf{0}\end{bmatrix}\begin{Bmatrix}\Delta\hat{\mathbf{H}}_m\\ \Delta\dot{\hat{\mathbf{H}}}_m\end{Bmatrix} + \begin{Bmatrix}\mathbf{0}\\ \Delta\ddot{\mathbf{H}}_m\end{Bmatrix} + \begin{bmatrix}\mathbf{L}_{ob1}\\ \mathbf{L}_{ob2}\end{bmatrix}\left\{\Delta\mathbf{H}_m - \Delta\hat{\mathbf{H}}_m\right\} \tag{29}
$$

where $\mathbf{L}_{ob1}$ and $\mathbf{L}_{ob2}$ are the Kalman filter gain matrices. Eq. (29) can also be expressed by:

$$
\begin{cases}
\Delta\dot{\hat{\mathbf{H}}}_m = \Delta\dot{\hat{\mathbf{H}}}_m - \mathbf{L}_{ob1}\Delta\hat{\mathbf{H}}_m + \mathbf{L}_{ob1}(\mathbf{N}_1\mathbf{Y}_m - \mathbf{U})\\
\Delta\ddot{\hat{\mathbf{H}}}_m = -\mathbf{L}_{ob2}\Delta\hat{\mathbf{H}}_m + \mathbf{L}_{ob2}(\mathbf{N}_1\mathbf{Y}_m - \mathbf{U}) + \mathbf{N}_1\ddot{\mathbf{Y}}_m - \ddot{\mathbf{U}}
\end{cases}
\tag{30}
$$

where $\mathbf{N}_1$ is the shape function matrix of the vehicle to solve the vertical displacements or accelerations, respectively.

2.2.4 State-Space Equation

All concerned expressions of the maglev vehicle with one car have been given so far. The mass matrix, stiffness matrix, damping matrix and coefficient matrices of fluctuating electromagnetic force in the equation of motion of the car have been assembled automatically based on the principle of virtual work. The coefficient matrices of governing equation of fluctuating current have been formed row by row in the computer program. An observer has been introduced to obtain both relative velocities and displacements related to the control currents. These three major coupled equations belong to differential equations with different orders. The conventional integral method does not directly address these three equations at the same time. Thus, a new state-space equation, including these three components, is derived. The 55-DOF car has 210 state variables, including 55 displacements of the rigid bodies and its first-order derivatives, 20 fluctuating currents, and 40 estimated vertical air gaps and its first-order derivatives, which can be expressed as following vector:

$$\mathbf{X} = [\mathbf{Y}_m, \dot{\mathbf{Y}}_m, \Delta\mathbf{I}_m, \Delta\hat{\mathbf{H}}_m, \Delta\dot{\hat{\mathbf{H}}}_m]^T \tag{31}$$

The coupled state-space equation of the maglev vehicle with one car is formed by:

Table 1. Main Vehicle System Parameters

Parameter	Unit	Value
Cabin body mass (m_c)	kg	23,292
Bogie mass (m_b)	kg	846
Roll inertia of cabin body (J_{cx})	kg m^2	66,800
Pitch inertia of cabin body (J_{cy})	kg m^2	210,000
Yaw inertia of cabin body (J_{cz})	kg m^2	193,000
Roll inertia of bogie (J_{bx})	kg m^2	963
Pitch inertia of bogie (J_{by})	kg m^2	1,800
Yaw inertia of bogie (J_{bz})	kg m^2	268
Longitudinal stiffness of secondary suspension (k_{cx})	N/m	900,000
Vertical stiffness of secondary suspension (k_{cy})	N/m	140,000
Lateral stiffness of secondary suspension (k_{cz})	N/m	6,000
Longitudinal damping of secondary suspension (c_{cx})	N s/m	50,000
Vertical damping of secondary suspension (c_{cy})	N s/m	70,000
Lateral damping of secondary suspension (c_{cz})	N s/m	4,000
Stiffness of spring-dampers connecting the left and right bogies (k_{by}, k_{bz})	N/m	4×10^8, 4,300
Damping of spring-dampers connecting the left and right bogies (c_{by}, c_{bz})	N s/m	1×10^6, 2,100
Resistance (R_0)	Ω	1.6
Air gap at balanced point (h_0)	mm	10
Pole area (A_0)	m^2	0.383
Coil turn (N_0)	-	660
Vacuum permeability (μ_0)	H/m	$4\pi \times 10^{-7}$
Width of electromagnet (d_0)	m	0.164
Length of cabin	m	16
Width of cabin	m	2.62
Height of cabin	m	2.9

$$\dot{\mathbf{X}} = \mathbf{AX} + \mathbf{BU} + \mathbf{C}\ddot{\mathbf{U}} + \mathbf{DV} \tag{32}$$

$$\mathbf{A} = \begin{bmatrix} \mathbf{0} & \mathbf{1} & \mathbf{0} & \mathbf{0} & \mathbf{0} \\ \mathbf{M}_m^{-1}\mathbf{A}_m - \mathbf{M}_m^{-1}\mathbf{K}_m & -\mathbf{M}_m^{-1}\mathbf{C}_m & \mathbf{M}_m^{-1}\mathbf{B}_m & \mathbf{0} & \mathbf{0} \\ \mathbf{D}_m\mathbf{M}_m^{-1}\mathbf{A}_m - \mathbf{D}_m\mathbf{M}_m^{-1}\mathbf{K}_m & -\mathbf{D}_m\mathbf{M}_m^{-1}\mathbf{C}_m & \mathbf{D}_m\mathbf{M}_m^{-1}\mathbf{B}_m + \mathbf{G}_m & \mathbf{O}_m & \mathbf{J}_m \\ \mathbf{L}_{ob1}\mathbf{N}_1 & \mathbf{0} & \mathbf{0} & -\mathbf{L}_{ob1} & \mathbf{1} \\ \mathbf{N}_1\mathbf{M}_m^{-1}\mathbf{A}_m - \mathbf{N}_1\mathbf{M}_m^{-1}\mathbf{K}_m + \mathbf{L}_{ob2}\mathbf{N}_1 & -\mathbf{N}_1\mathbf{M}_m^{-1}\mathbf{C}_m & \mathbf{N}_1\mathbf{M}_m^{-1}\mathbf{B}_m & -\mathbf{L}_{ob2} & \mathbf{0} \end{bmatrix} \tag{33}$$

$$\mathbf{B} = \begin{bmatrix} \mathbf{0} \\ \mathbf{M}_m^{-1}\mathbf{E}_m \\ \mathbf{D}_m\mathbf{M}_m^{-1}\mathbf{E}_m \\ -\mathbf{L}_{ob1} \\ \mathbf{N}_1\mathbf{M}_m^{-1}\mathbf{E}_m - \mathbf{L}_{ob2} \end{bmatrix} \tag{34}$$

$$\mathbf{C} = \begin{bmatrix} \mathbf{0} \\ \mathbf{0} \\ \mathbf{0} \\ \mathbf{0} \\ \mathbf{I} \end{bmatrix} \tag{35}$$

$$\mathbf{D} = \begin{bmatrix} \mathbf{0} \\ \mathbf{M}_m^{-1}\mathbf{Q}_m \\ \mathbf{D}_m\mathbf{M}_m^{-1}\mathbf{Q}_m \\ \mathbf{0} \\ \mathbf{N}_1\mathbf{M}_m^{-1}\mathbf{Q}_m \end{bmatrix} \tag{36}$$

2.3 State-Space Equations of Multicar Maglev Vehicles

The left- and right-hand maglev vehicles travel along on their own lines. The maglev vehicles-bridge interaction model is required to share a global Cartesian coordinate system in the process of calculation. In this study, all local coordinate systems of the left-hand maglev vehicle are parallel to the global coordinate system, and their directions are also same. For the left-hand maglev vehicle with many of the same cars, the state-space equation of each car still has the same state matrix and input matrices. However, the input vectors from both bridge motions and track irregularities and the output vector of each car should be different due to the different traveling positions of cars on the guideway. Based on Eq. (32), the state-space equation of the left-hand vehicle with n cars can be described by:

$$\begin{Bmatrix} \dot{\mathbf{X}}_{lt1} \\ \dot{\mathbf{X}}_{lt2} \\ \vdots \\ \dot{\mathbf{X}}_{ltn} \end{Bmatrix} = \begin{bmatrix} \mathbf{A}_{lt} & & & \\ & \mathbf{A}_{lt} & & \\ & & \ddots & \\ & & & \mathbf{A}_{lt} \end{bmatrix} \begin{Bmatrix} \mathbf{X}_{lt1} \\ \mathbf{X}_{lt2} \\ \vdots \\ \mathbf{X}_{ltn} \end{Bmatrix} + \begin{bmatrix} \mathbf{B}_{lt} & & & \\ & \mathbf{B}_{lt} & & \\ & & \ddots & \\ & & & \mathbf{B}_{lt} \end{bmatrix} \begin{Bmatrix} \mathbf{U}_{lt1} \\ \mathbf{U}_{lt2} \\ \vdots \\ \mathbf{U}_{ltn} \end{Bmatrix} + \begin{bmatrix} \mathbf{C}_{lt} & & & \\ & \mathbf{C}_{lt} & & \\ & & \ddots & \\ & & & \mathbf{C}_{lt} \end{bmatrix} \begin{Bmatrix} \ddot{\mathbf{U}}_{lt1} \\ \ddot{\mathbf{U}}_{lt2} \\ \vdots \\ \ddot{\mathbf{U}}_{ltn} \end{Bmatrix} + \begin{bmatrix} \mathbf{D}_{lt} & & & \\ & \mathbf{D}_{lt} & & \\ & & \ddots & \\ & & & \mathbf{D}_{lt} \end{bmatrix} \begin{Bmatrix} \mathbf{V}_{lt1} \\ \mathbf{V}_{lt2} \\ \vdots \\ \mathbf{V}_{ltn} \end{Bmatrix} \tag{37}$$

where $\mathbf{X}_{ltn}$ is the state vector of the state-space equation for the nth car in the left-hand maglev vehicle, $\mathbf{U}_{ltn}$, $\ddot{\mathbf{U}}_{ltn}$ and $\mathbf{V}_{ltn}$ are the corresponding input vectors, and $\mathbf{A}_{lt}$, $\mathbf{B}_{lt}$, $\mathbf{C}_{lt}$ and $\mathbf{D}_{lt}$ are the corresponding coefficient matrices. For the right-hand maglev vehicle, all longitudinal and lateral directions in local coordinates

are completely opposite to the global coordinate. The transform matrix T_m from the local coordinates in the right-hand vehicles to the global coordinate is required, and it can be expressed as:

$$T_m = \begin{bmatrix} -1 & & \\ & 1 & \\ & & -1 \end{bmatrix} \tag{38}$$

In a similar way to deal with the right-hand maglev vehicle with n cars, the state-space equation can also be given as the following form with the help of the transform matrix.

$$\begin{Bmatrix} \dot{\mathbf{X}}_{rt1} \\ \dot{\mathbf{X}}_{rt2} \\ \vdots \\ \dot{\mathbf{X}}_{rtn} \end{Bmatrix} = \begin{bmatrix} \mathbf{A}_{rt} & & & \\ & \mathbf{A}_{rt} & & \\ & & \ddots & \\ & & & \mathbf{A}_{rt} \end{bmatrix} \begin{Bmatrix} \mathbf{X}_{rt1} \\ \mathbf{X}_{rt2} \\ \vdots \\ \mathbf{X}_{rtn} \end{Bmatrix} + \begin{bmatrix} \mathbf{B}_{rt} & & & \\ & \mathbf{B}_{rt} & & \\ & & \ddots & \\ & & & \mathbf{B}_{rt} \end{bmatrix} \begin{Bmatrix} \mathbf{U}_{rt1} \\ \mathbf{U}_{rt2} \\ \vdots \\ \mathbf{U}_{rtn} \end{Bmatrix}$$
$$+ \begin{bmatrix} \mathbf{C}_{rt} & & & \\ & \mathbf{C}_{rt} & & \\ & & \ddots & \\ & & & \mathbf{C}_{rt} \end{bmatrix} \begin{Bmatrix} \ddot{\mathbf{U}}_{rt1} \\ \ddot{\mathbf{U}}_{rt2} \\ \vdots \\ \ddot{\mathbf{U}}_{rtn} \end{Bmatrix} + \begin{bmatrix} \mathbf{D}_{rt} & & & \\ & \mathbf{D}_{rt} & & \\ & & \ddots & \\ & & & \mathbf{D}_{rt} \end{bmatrix} \begin{Bmatrix} \mathbf{V}_{rt1} \\ \mathbf{V}_{rt2} \\ \vdots \\ \mathbf{V}_{rtn} \end{Bmatrix} \tag{39}$$

in which $\mathbf{X}_{rtn}$ is the state vector of the state-space equation for the nth car in the right-hand maglev vehicles, $\mathbf{U}_{rtn}$, $\ddot{\mathbf{U}}_{rtn}$ and $\mathbf{V}_{rtn}$ are the corresponding input vectors, and $\mathbf{A}_{rt}$, $\mathbf{B}_{rt}$, $\mathbf{C}_{rt}$ and $\mathbf{D}_{rt}$ are the corresponding coefficient matrices.

3. Model of the Bridge

3.1 Equation of Motion of the Bridge

A real continuous girder bridge with three spans in the CME is considered as the guideway girder model shown in Fig. 3. The long-span continuous girder bridge has a total length of 280 m with the main span measured at 110 m and the two side spans of 85 m. The bridge is variable cross-section concrete girder with single box. The origin of global coordinate system of the maglev vehicles-bridge system is located at the left-hand endpoint of the bridge and the x-, y- and z-axes are expressed as the longitudinal, vertical and lateral directions, respectively, which follows the right-hand rule. When two maglev vehicles intersect at the bridge midpoint P_3, the mid-section of the mid-span is illustrated in Fig. 4. P_1 and P_2 are the left- and right-hand endpoints of the bridge, respectively. By using 3D Euler-Bernoulli beam elements to establish the 3D finite element model of the bridge (Logan, 2011), the equation of motion is given as:

$$\mathbf{M}_{br}\ddot{\mathbf{Y}}_{br} + \mathbf{C}_{br}\dot{\mathbf{Y}}_{br} + \mathbf{K}_{br}\mathbf{Y}_{br} = \mathbf{F}_{br} \tag{40}$$

where $\mathbf{Y}_{br}$ is the bridge displacement vector, $\mathbf{M}_{br}$ and $\mathbf{K}_{br}$ are the mass and stiffness matrices of the bridge, $\mathbf{C}_{br}$ is the Rayleigh damping matrix and the damping ratios of the bridge are 0.03, and $\mathbf{F}_{br}$ is the time-dependent node vector of the electromagnetic force.

$$\mathbf{F}_{br} = \mathbf{N}_4(\mathbf{G}_{br} + k_i\mathbf{N}_2\mathbf{X}_{lt} + k_h\mathbf{N}_1\mathbf{X}_{lt} - k_h\mathbf{U}_{lt}) + \mathbf{N}_5(k_e\mathbf{N}_3\mathbf{X}_{lt} - k_e\mathbf{V}_{lt})$$
$$+\mathbf{N}_6(\mathbf{G}_{br} + k_i\mathbf{N}_2\mathbf{X}_{rt} + k_h\mathbf{N}_1\mathbf{X}_{rt} - k_h\mathbf{U}_{rt}) + \mathbf{N}_7(k_e\mathbf{N}_3\mathbf{X}_{rt} - k_e\mathbf{V}_{rt}) \tag{41}$$

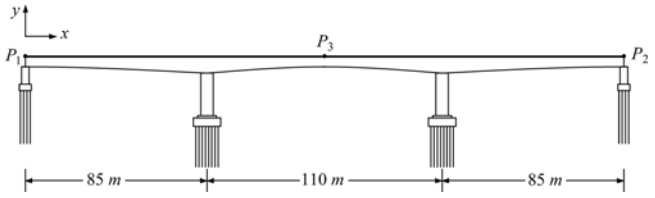

Fig. 3. Model of the Three-Span Continuous Girder Bridge

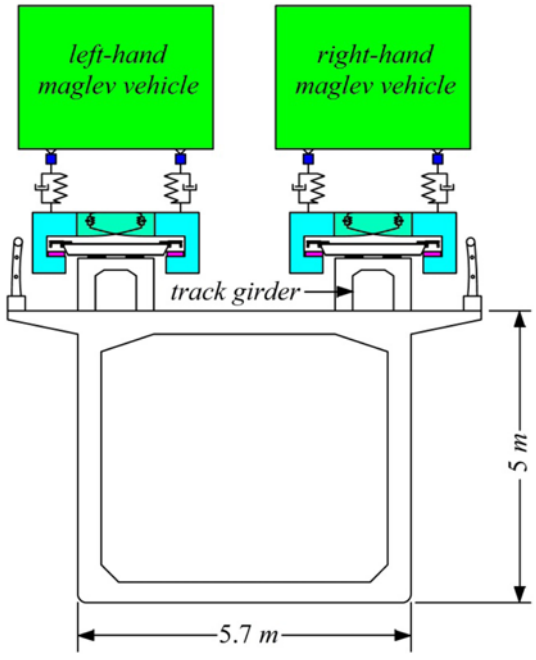

Fig. 4. Typical Cross-Section of Bridge when Vehicles Intersect at Midpoint P_3

where, $\mathbf{X}_{lt} = [\mathbf{X}_{lt1}, \mathbf{X}_{lt2}, \cdots, \mathbf{X}_{ltn}]^T$, $\mathbf{U}_{lt} = [\mathbf{U}_{lt1}, \mathbf{U}_{lt2}, \cdots, \mathbf{U}_{ltn}]^T$, $\mathbf{V}_{lt} = [\mathbf{V}_{lt1}, \mathbf{V}_{lt2}, \cdots, \mathbf{V}_{ltn}]^T$, $\mathbf{X}_{rt} = [\mathbf{X}_{rt1}, \mathbf{X}_{rt2}, \cdots, \mathbf{X}_{rtn}]^T$, $\mathbf{U}_{rt} = [\mathbf{U}_{rt1}, \mathbf{U}_{rt2}, \cdots, \mathbf{U}_{rtn}]^T$, $\mathbf{V}_{rt} = [\mathbf{V}_{rt1}, \mathbf{V}_{rt2}, \cdots, \mathbf{V}_{rtn}]^T$, $\mathbf{N}_4$, $\mathbf{N}_5$, $\mathbf{N}_6$ and $\mathbf{N}_7$ are the time-dependent matrices used to obtain the bridge node forces; $\mathbf{N}_2$ and $\mathbf{N}_3$ denote the matrices used to attain the fluctuating currents and lateral displacements, respectively; and $\mathbf{G}_{br}$ is the vector of the equivalent gravity and each element in the vector equals to the G_0.

The guideway displacements in Eq. (41) can be expressed by following forms:

$$\mathbf{U}_{lt} = \mathbf{N}_8\mathbf{Y}_{br} + \mathbf{R}_{ltu} \tag{42}$$

$$\mathbf{V}_{lt} = \mathbf{N}_9\mathbf{Y}_{br} + \mathbf{R}_{ltv} \tag{43}$$

$$\mathbf{U}_{rt} = \mathbf{N}_{10}\mathbf{Y}_{br} + \mathbf{R}_{rtu} \tag{44}$$

$$\mathbf{V}_{rt} = \mathbf{N}_{11}\mathbf{Y}_{br} + \mathbf{R}_{rtv} \tag{45}$$

Here, $\mathbf{R}_{ltu}$ and $\mathbf{R}_{ltv}$ are the vertical and lateral guideway irregularities of the left-hand maglev vehicle, $\mathbf{R}_{rtu}$ and $\mathbf{R}_{rtv}$ are the vertical and lateral guideway irregularities of the right-hand maglev vehicle, and $\mathbf{N}_8$, $\mathbf{N}_9$, $\mathbf{N}_{10}$ and $\mathbf{N}_{11}$ are the time-dependent shape function matrices used to obtain the bridge displacements. $\mathbf{N}_4$, $\mathbf{N}_5$, $\mathbf{N}_8$ and $\mathbf{N}_9$ are the functions of the left-hand maglev

vehicle at the traveling distances $x_{lt} = V_{lt}t - S_{lt}$, and $\mathbf{N}_6$, $\mathbf{N}_7$, $\mathbf{N}_{10}$ and $\mathbf{N}_{11}$ are the functions of the right-hand maglev vehicle at the traveling distances $x_{rt} = -V_{rt}t + l_{br} + S_{rt}$, in which S_{lt} and S_{rt} are the distances from the first electromagnetic force of the left- and right-hand maglev vehicles to the bridge, respectively; l_{br} is the total length of the bridge; t is the traveling time of the maglev vehicles. Furthermore, the second-order derivative of the vertical guideway displacements in Eqs. (38) and (39) can be further expressed by:

$$\ddot{\mathbf{U}}_{lt} = V_{lt}^2 \frac{\partial^2 \mathbf{N}_8}{\partial x_{lt}^2}\mathbf{Y}_{br} + 2V_{lt}\frac{\partial \mathbf{N}_8}{\partial x_{lt}}\dot{\mathbf{Y}}_{br} + \mathbf{N}_8\ddot{\mathbf{Y}}_{br} + V_{lt}^2\frac{\partial^2 \mathbf{R}_{ltu}}{\partial x_{lt}^2} \quad (46)$$

$$\ddot{\mathbf{U}}_{rt} = V_{rt}^2 \frac{\partial^2 \mathbf{N}_{10}}{\partial x_{rt}^2}\mathbf{Y}_{br} - 2V_{rt}\frac{\partial \mathbf{N}_{10}}{\partial x_{rt}}\dot{\mathbf{Y}}_{br} + \mathbf{N}_{10}\ddot{\mathbf{Y}}_{br} + V_{rt}^2\frac{\partial^2 \mathbf{R}_{rtu}}{\partial x_{rt}^2} \quad (47)$$

3.2 Guideway Irregularity

Guideway irregularity plays an important role in inducing the vibration for the maglev vehicle-bridge interaction (Ren et al., 2010). In the 3D direction, there are four types of guideway irregularities, such as elevation, super-elevation, alignment and gauge irregularities (Frýba, 1996; Yang et al., 2004). Elevation and alignment irregularities are derivations of centerlines of parallel rails from the ideal geometry of track layout in vertical and lateral directions while super-elevation and gauge irregularities denote the differences in elevations and horizontals of parallel rails. These derivations with frequency characteristics can be manifested via the power spectral density (PSD) functions. In this study, irregularity characteristics of two parallel F-shaped rails on the bridge is described through the following PSD functions (Frýba, 1996).

$$S_1(\Omega) = \frac{C_1\Omega_1^2}{(\Omega^2+\Omega_2^2)(\Omega^2+\Omega_1^2)} \quad (48)$$

$$S_2(\Omega) = \frac{C_1 b_h^{-2}\Omega_1^2\Omega^2}{(\Omega^2+\Omega_1^2)(\Omega^2+\Omega_2^2)(\Omega^2+\Omega_3^2)} \quad (49)$$

$$S_3(\Omega) = \frac{C_2\Omega_1^2}{(\Omega^2+\Omega_2^2)(\Omega^2+\Omega_1^2)} \quad (50)$$

$$S_4(\Omega) = \frac{C_3\Omega_1^2\Omega^2}{(\Omega^2+\Omega_1^2)(\Omega^2+\Omega_2^2)(\Omega^2+\Omega_3^2)} \quad (51)$$

where Ω_1 (= 0.8246 rad/m), Ω_2 (= 0.0206 rad/m) and Ω_3 (= 0.438 rad/m) are the cut-off frequencies, C_1 (= 1.5 × 10^{-7} m^2/rad/m), C_2 (= 0.6 × 10^{-7} m^3/rad) and C_3 (= 14 × 10^{-8} m^3/rad) are the roughness constants, b_h is the half-length of the width of the parallel rails, and Ω (rad/m) denotes the spatial angular frequency. Assuming that the guideway irregularities are zero-mean stationary Gaussian random processes, the distance history of deviations $R(x)$ can be described by (Goller et al., 2013):

$$R(x) = \sum_{k=1}^{N}\sqrt{2S(\Omega)\Delta\Omega}\cos(\Omega x + \theta_k) \quad (52)$$

where θ_k is the phase angle at the kth sample, which is the random variation ranging from 0 to 2π. In this way, the deviations of these four types of guideway irregularities for the left-hand and right-hand parallel rails are expressed as $\mathbf{R}_1(x)$, $\mathbf{R}_2(x)$, $\mathbf{R}_3(x)$ and $\mathbf{R}_4(x)$, as well as $\mathbf{R}_5(x)$, $\mathbf{R}_6(x)$, $\mathbf{R}_7(x)$ and $\mathbf{R}_8(x)$, respectively. Thus, the guideway irregularities in Eqs. (42) – (45) can be given by:

$$\mathbf{R}_{ltu} = [\mathbf{R}_1 + b_h\mathbf{R}_3, \mathbf{R}_1 - b_h\mathbf{R}_3] \quad (53)$$

$$\mathbf{R}_{ltv} = [\mathbf{R}_2 - \mathbf{R}_4/2, \mathbf{R}_4 + \mathbf{R}_4/2] \quad (54)$$

$$\mathbf{R}_{rtu} = [\mathbf{R}_5 + b_h\mathbf{R}_7, \mathbf{R}_5 - b_h\mathbf{R}_7] \quad (55)$$

$$\mathbf{R}_{rtv} = [\mathbf{R}_6 - \mathbf{R}_8/2, \mathbf{R}_6 + \mathbf{R}_8/2] \quad (56)$$

Here, each matrix of guideway irregularities contains the parallel two rails. The lengths of these guideway irregularities are the distance from P_1 to P_2 points (see Fig. 3). For instance, the vertical guideway irregularities for the left-hand vehicle and its second-order derivative are shown in Fig. 5.

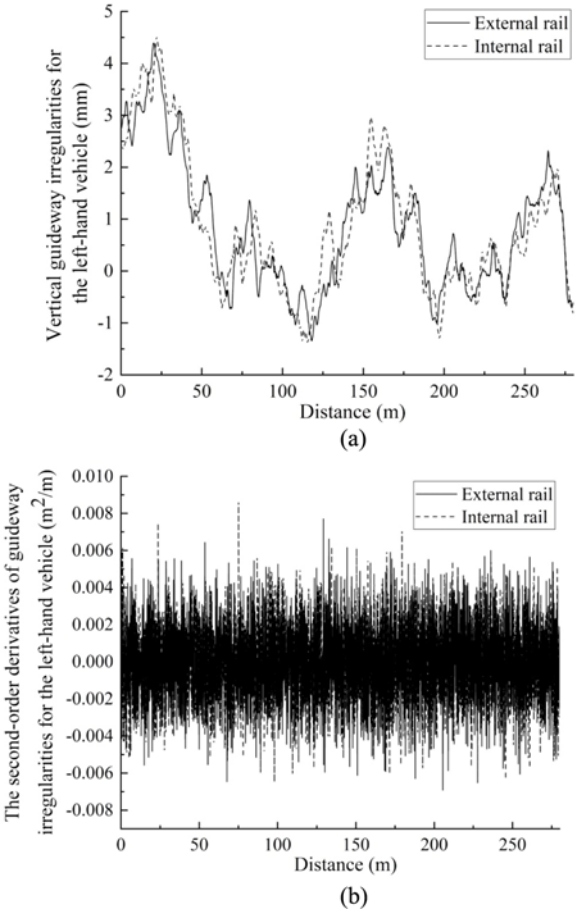

Fig. 5. Guideway Irregularity of the Left-Hand Vehicle in: (a) The Vertical Direction, (b) Its Second-Order Derivative

4. Iteration Approach for Coupled Equations

In this study, for the model of the long-span continuous girder bridge with double lines subjected the moving maglev vehicles,

there are two types of equations: two state-space equations for the left- and right-hand maglev vehicles and the other equation of motion of the bridge. Without the effect of the external environment, the interactions are produced between maglev vehicles and the bridge via electromagnetic forces, and the direct interactions do not exist between two maglev vehicles. A new effective iteration method is applied to solve the coupled equations of the maglev vehicles-bridge system. During the iteration, the node displacements of the bridge are assumed first. Based on the precise integration method (Zhang et al., 2010), the response results of two maglev vehicles are then computed to obtain the electromagnetic forces acting on the bridge. By using the Newmark-β method (Newmark, 1959), bridge displacements are solved to compare with results before iteration. This iteration will be ceased only if the displacements of all bridge nodes from the two consecutive iterations are close enough. The detailed iteration process is given as Fig. 6. It should be emphasized that assumed displacements of the initial iteration at each time step are set to be displacement results of the bridge at the last time step to ensure the efficiency of iteration.

Eventually, the model of the three-span space continuous girder bridge under the same two moving multicar maglev vehicles has been built, and the associated computer program has also been completed. The model and corresponding computer program have accomplished some automatic operations: 1) the major matrices of the maglev vehicles-bridge system can be assembled conveniently; 2) any number of cars in the maglev vehicles can be obtained by means of the parameter n; 3) the required positions of two maglev vehicles with different traveling speeds on the guideway can be decided by changing the parameters V_{lt}, V_{rt}, S_{lt} and S_{rt}; and 4) the case of only one maglev vehicle moving on the bridge is easily realized by setting the traveling speed of the other maglev vehicle as zero.

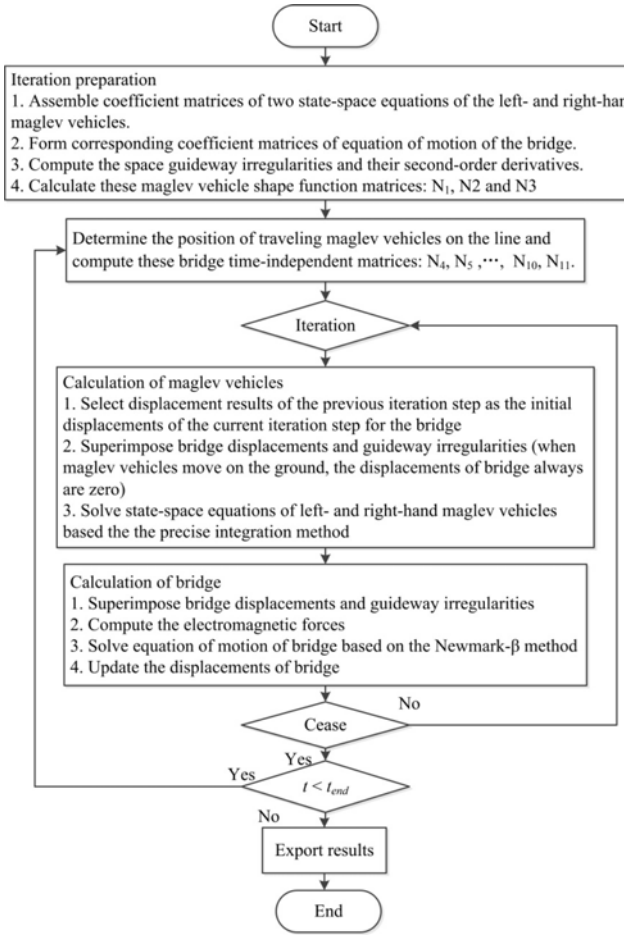

Fig. 6. Flow Chart of the Iterative Procedure

5. Numerical Results

5.1 Verification of Correctness

To verify the correctness of the established 3D model of maglev vehicles traveling over the continuous girder bridge in this study, the time histories of cabin vertical displacements for left- and

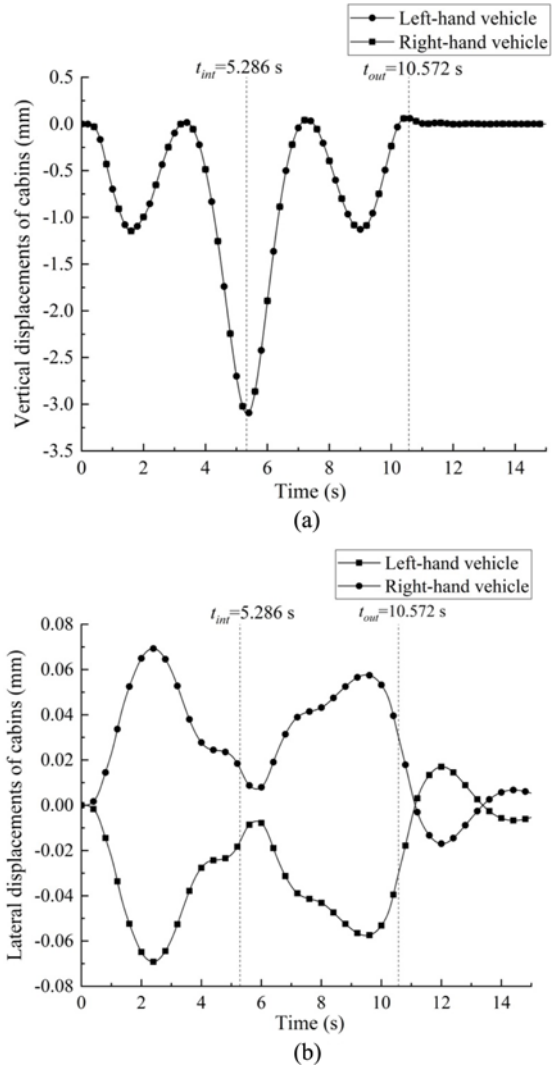

Fig. 7. Displacement Responses of Cabins in: (a) Vertical, (b) Lateral Directions when Maglev Vehicles with the Speeds of 100 km/h Pass by Each Other on the Bridge

right-hand maglev vehicles should be exactly the same, and their lateral displacements ought to be completely opposite when two maglev vehicles at the same speed pass by each other on the three-span continuous girder bridge with smooth guideways. These requirements are because the continuous girder bridge is a symmetrical structure and two sets of maglev vehicles have the same properties. The response curves of the vertical and lateral displacements of the cabins for the two vehicles with one car as shown in Fig. 7, meet the requirements. In this case, the parameters S_{lt} and S_{rt} are set to zero and traveling speeds of the vehicles are 100 km/h. The t_{int} = 5.286 s is the time when two vehicles happen to intersect at the bridge midpoint P_3, and they leave the bridge at the time of t_{out} = 10.572 s.

Another main requirement is that the minimum displacement of the bridge midpoint under the condition of only one traveling maglev vehicle should be half of that of two maglev vehicles passing by each other because the continuous girder bridge is assumed to be a linear structure, and its deformations are smaller. Fig. 8(a) shows the time history of the bridge at point P_3 in these two conditions, and corresponding minimum displacements are 1.52 and 3.04 mm, respectively. Moreover, the lateral displacement of the bridge midpoint under the two passing maglev vehicles can be negligible compared to only one traveling maglev vehicle because guide loads acting on the bridge for the left- and right-hand maglev vehicles are just opposite (see Fig. 8(b)). In summary, the correctness of these requirements has the ability to verify the proposed 3D model of two maglev vehicles traveling over the three-span continuous girder bridge.

5.2 Effect of Guideway Irregularity

In this section, the cars of the maglev vehicles are set as three based on the practical condition. The left-hand maglev vehicle and the opposite right-hand maglev vehicle begin to move at P_1 and P_2 points respectively at the same speed of 100 km/h, and they happen to intersect at the point P_3. Displayed in Fig. 9 are the vertical and lateral acceleration curves of the second cabin of the left-hand maglev vehicle in the two cases of the smooth guideways and irregularity guideways. The second car of the

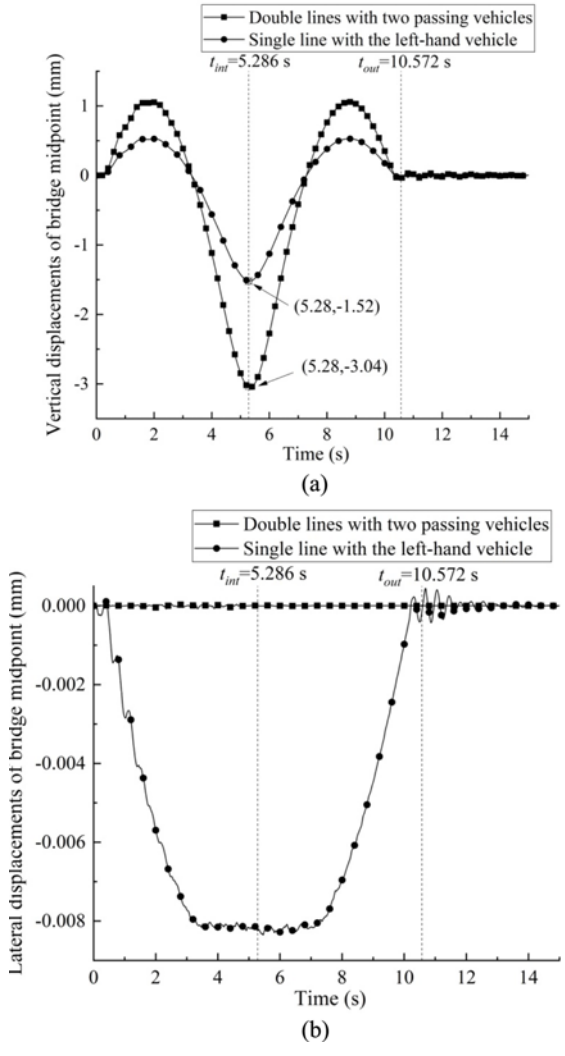

Fig. 8. Displacement Responses of the Point P_3 of the Bridge in: (a) Vertical, (b) Lateral Directions with Two Cases of the Double Lines and Single Line

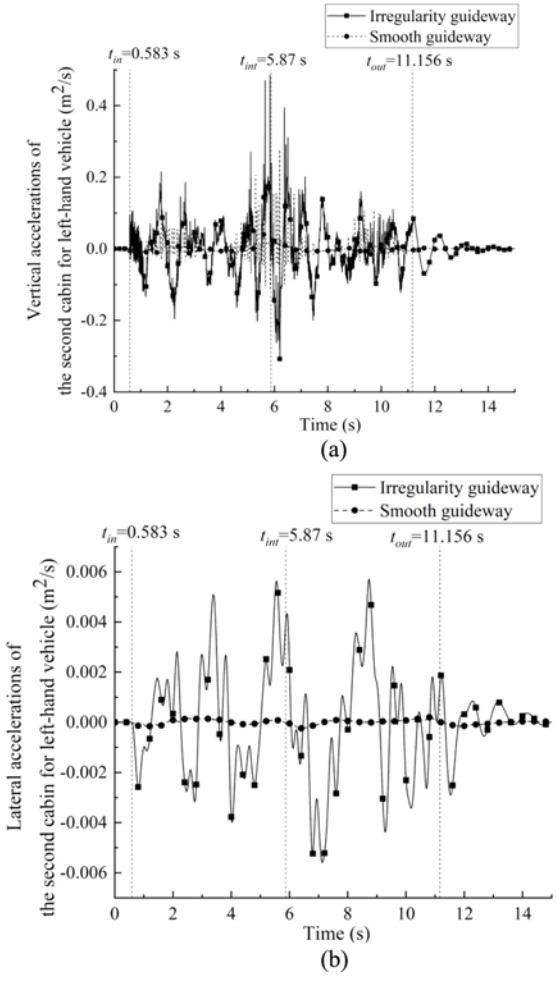

Fig. 9. Acceleration Responses of the Second Cabin for: (a) Vertical, (b) Lateral Directions in Two Cases of Irregularity and Smooth Guideways

left-hand vehicle moves on the bridge at time range from t_{in} = 0.583 s to t_{out} = 11.156 s, and the time t_{int} = 5.87 s is the intersecting moment of the two vehicles. Compared to the lateral acceleration, the second cabin acceleration in the vertical direction is associated with the positions of maglev vehicles on the bridge, in which the vertical accelerations for the positions of maglev vehicles around the midpoints of three spans on the bridge are much larger than the other positions on the bridge. Certainly, the maximum response exists around the bridge midpoint P_3. It can also be seen that the effects of guideway irregularities on the cabin motions are great in the whole process of maglev vehicles moving on the bridge, especially for the lateral acceleration mainly depending on the lateral guideway irregularities.

In addition, when two maglev vehicles arrive around the bridge midpoint P_3, the vertical acceleration responses of midpoint P_3 increase significantly (see Fig. 10(a)). For the bridge with smooth guideways under the vehicles passing by each other, little lateral vibrations of the bridge occur first, but these vibrations soon tend to zero before vehicles leave the bridge due to the bridge subjected to a series of opposite lateral loads from the maglev vehicles (see Fig. 10(b)). This phenomenon is consistent with the observation from Fig. 8(b). We can conclude that lateral dynamic responses of the maglev vehicles-bridge system are decided by the lateral guideway irregularities for the two sets of maglev vehicles with same speeds passing over the bridge. Even if guideway irregularities have a great influence on the vertical and lateral acceleration responses of the maglev vehicles-bridge system, the vertical accelerations still are much larger than the lateral accelerations. As a result, the vertical motions dominate the dynamic behaviors of the maglev vehicles-bridge interaction system due to very large lateral stiffness of the bridge in this case study.

5.3 Effect of Traveling Speeds of Maglev Vehicles

Displayed in Fig. 11 are the maximum values of the vertical and lateral accelerations of the second cabin of the left-hand vehicle in two cases of double lines and single line. With the increase in the traveling speed of maglev vehicles, the maximum responses of the second cabin accelerations in the vertical and lateral

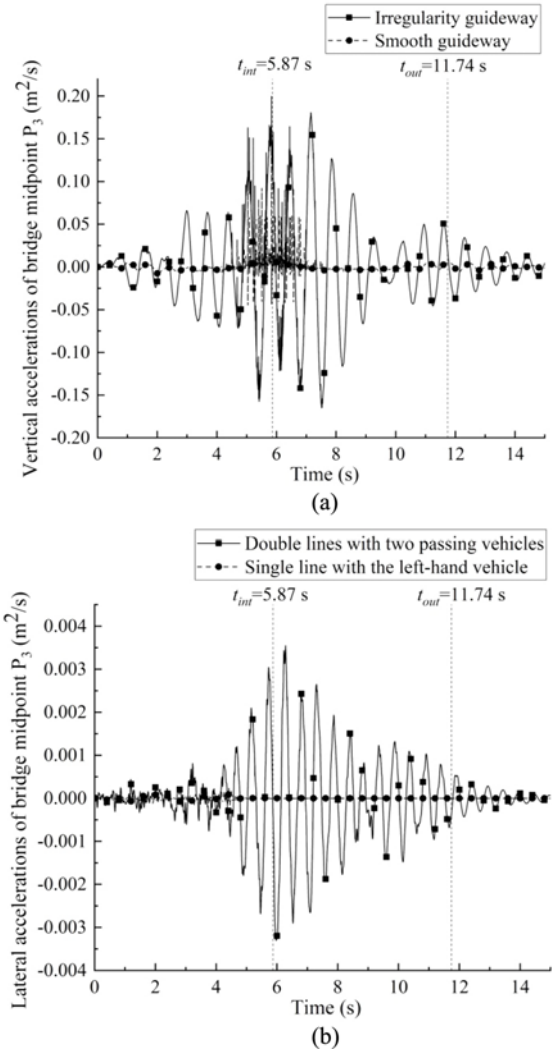

Fig. 10. Acceleration Responses of the Bridge Midpoint P_3 for: (a) Vertical, (b) Lateral Directions in Two Cases of Irregularity and Smooth Guideways

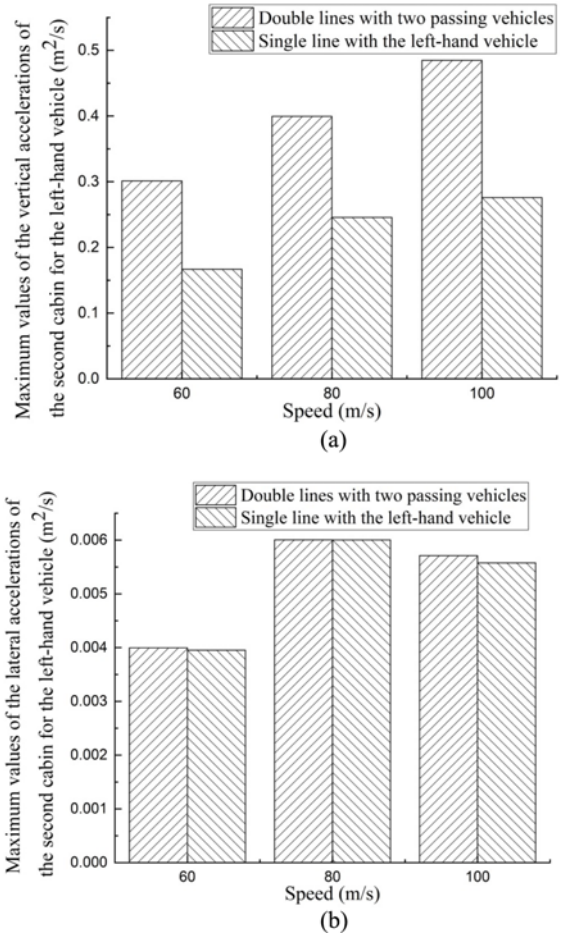

Fig. 11. Effect of Vehicle Speeds on the Maximum Values of: (a) Vertical, (b) Lateral Accelerations of the Second Cabin for the Left-Hand Vehicle

directions increase slightly. Moreover, the maximum responses of the second cabin acceleration in the lateral direction are almost the same for the double lines and single line. This observation may be because the lateral stiffness of the continuous bridge is large enough, and the passing vehicle on the other side line has little influence such that the lateral accelerations of the maglev vehicles are mainly affected by their own guideway irregularities and traveling speeds. For the vertical accelerations of the cabin at different traveling speeds, the maximum responses for the double lines are slightly less than the twice that of the single line.

On the other hand, the maximum values of the vertical accelerations for the bridge midpoint P_3 increase with increasing maglev vehicle traveling speeds when only the left-hand vehicle moves on the bridge, but its lateral accelerations have no variety (see Fig. 12). The single line of the left-hand vehicle with different given traveling speeds influenced by guideway irregularities has difficulty in inducing a change in the lateral maximum accelerations of the bridge midpoint P_3. However, the double lines of two passing maglev vehicles can achieve this change, but the specific regularity between vehicles traveling speeds and maximum acceleration of the bridge midpoint P_3 is not observed. The reason may be the random characteristics of the guideway irregularities for two maglev vehicles traveling along the bridge with double lines.

5.4 Effect of Cars in Maglev Vehicles

With the increased number of cars in the maglev vehicles, the minima of vertical displacements in the midpoint P_3 of the bridge with double lines decrease gradually and then tend to be stable after the number of cars exceeds 4 (see Fig. 13(a)). Meanwhile, for the bridge with a single line of only the moving left-hand vehicle, the vertical displacements for the bridge midpoint P_3 have a similar tendency. In these cases, the traveling speeds of the maglev vehicles are 100 km/h. Note that the number 4 is less than 6.88, which is the result of the length of the bridge main span divided by the length of the car. Displayed in Fig. 13(b) are the minimum lateral displacements of the bridge midpoint P_3 under different numbers of cars. Fig. 13(b) shows that the lateral deformation of the bridge midpoint P_3 for the single line is always greater than for the double lines. In addition, the lateral deformation of bridge under single line increases with increasing numbers of cars. When the number of cars is fewer than 4, the differences in the minimum lateral displacements between

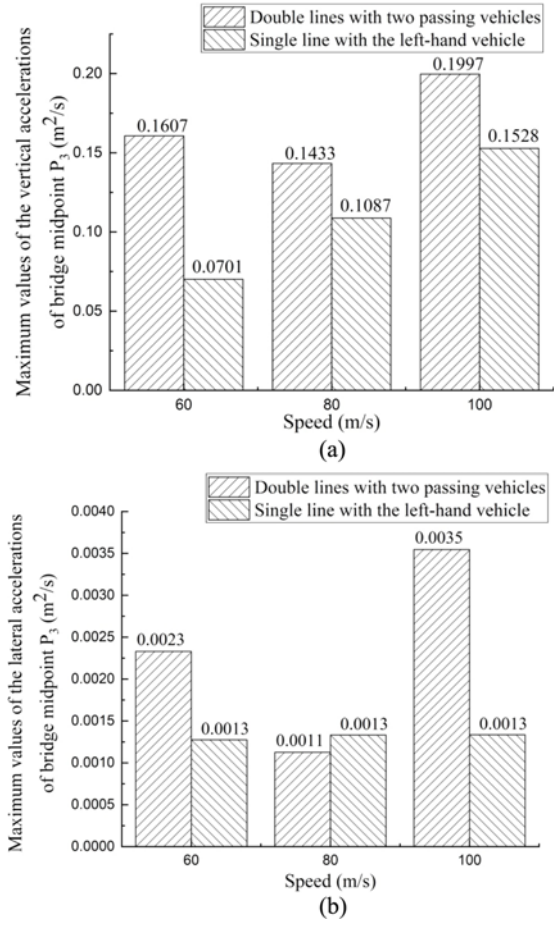

Fig. 12. Effect of Vehicle Speeds on the Maximum Values of: (a) Vertical, (b) Lateral Accelerations of the Bridge Midpoint P_3

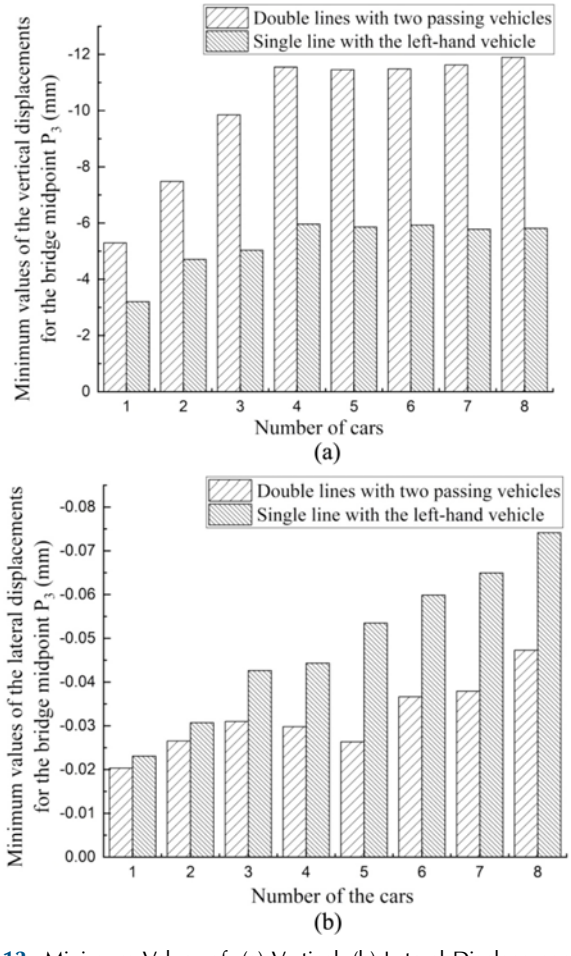

Fig. 13. Minimum Values of: (a) Vertical, (b) Lateral Displacements of the Bridge Midpoint P_3 for the Different Cars in Maglev Vehicles

double lines and the single line increase as the number of cars in the vehicles increases.

6. Conclusions

This paper established a complete 3D model of maglev vehicles traveling over a three-span continuous girder bridge. The model considered the dynamic behaviors of maglev vehicles, control currents, linear feedback control systems, estimations of unmeasured variables, motions of a space continuous girder bridge with double lines and vertical and lateral guideway irregularities. The major conclusions based on numerical simulations of the poposed model can be drawn as follows:

1. The vertical motions dominate the dynamic behavior of the maglev vehicles-bridge interaction and the lateral motions of the vehicle are unaffected by the traveling maglev vehicle on the other line due to the large lateral stiffness of the bridge.
2. The guideway irregularities have a great effect on the dynamic responses of the maglev vehicles-bridge system, and the lateral motions of two passing vehicles on the bridge depend on the lateral guideway irregularities.
3. With the increase in the traveling speeds, the maximum vertical and lateral accelerations of the vehicle have the increasing tendency under the bridge with single line and double lines, but the maximum lateral accelerations for the bridge midpoint P_3 with single line show little change.
4. The deformations of vertical displacements for the bridge midpoint P_3 under double lines are always larger than that of single lines with the increase in the number of cars in maglev vehicles, while its lateral displacements have an opposite regularity.

The above conclusions of the numerical simulation using the proposed 3D coupled model are drawn based on a specific case study, and more general regularity is needed to conduct many further tests of numerical simulations for different types of bridge.

Acknowledgements

This research is support by the National Natural Science Foundation of China (Project No. 51078356), and the Major Technology Research and Development Program of Ministry of Railway of China (Project No. 2008G031-Q).

ORCID

Wei Liu https://orcid.org/0000-0003-2734-6952
WenHua Guo https://orcid.org/0000-0003-0051-3837

References

Cai Y, Chen SS (1997) Dynamic characteristics of magnetically-levitated vehicle systems. *Applied Mechanics Review* 50(11):647-670, DOI: 10.1115/1.3101676

Cai Y, Chen SS, Rote DM (1992) Dynamics and controls in maglev systems. NO. ANL-92/43, Argonne National Laboratory, Lemont, IL, USA

Cai Y, Chen SS, Rote DM, Coffey HT (1994) Vehicle/guideway interaction for high speed vehicles on a flexible guideway. *Journal of Sound and Vibration* 175(5):625-646, DOI: 10.1006/jsvi.1994.1350

Frýba L (1996) Dynamics of railway bridges. Thomas Telford Publishing, London, UK, 120-125

Glatzel K, Khurdok G, Rogg D (1980) The development of the magnetically suspended transportation system in the federal republic of germany. *IEEE Transactions on Vehicular Technology* 29(1):3-17, DOI: 10.1109/T-VT.1980.23816

Goller B, Pradlwarter HJ, Scuëller GI (2013) Reliability assessment in structural dynamics. *Journal of Sound and Vibration* 332:2488-2499, DOI: 10.1016/j.jsv.2012.11.021

Kaloust J, Ham C, Siehling J, Jongkryg E, Han Q (2004) Nonlinear robust control design for levitation and propulsion of a maglev system. *IEE Proceedings - Control Theory and Applications* 151(4):460-464, DOI: 10.1049/ip-cta:20040547

Kim KJ, Han JB, Han HS, Yang SJ (2015) Coupled vibration analysis of maglev vehicle-guideway while standing still or moving at low speeds. *Vehicle System Dynamics* 53(4):587-601, DOI: 10.1080/00423114.2015.1013039

Kong E, Song JS, Kang BB, Na S (2011) Dynamic response and robust control of coupled maglev vehicle and guideway system. *Journal of Sound and Vibration* 330(25):6237-6253, DOI: 10.1016/j.jsv.2011.05.031

Kwon SD, Lee JS, Moon JW, Kim MY (2008) Dynamic interaction analysis of urban transit maglev vehicle and guideway suspension bridge subjected to gusty wind. *Engineering Structures* 30(12):3445-3456, DOI: 10.1016/j.engstruct.2008.05.003

Liu W, Guo WH (2019) Random vibration analysis of coupled three-dimensional maglev vehicle-bridge System. *Advances in Civil Engineering* 2019:1-14, DOI: 10.1155/2019/4920659

Logan DL (2011) A first course in the finite element method. Cengage Learning, Boston, MA, USA, 277-280

Min DJ, Jung MR, Kim MY, Kwark JW (2017) Dynamic interaction analysis of maglev-guideway system based on a 3D full vehicle model. *International Journal of Structural Stability and Dynamics* 17(01):1750006, DOI: 10.1142/S0219455417500067

Newmark NM (1959) A method of computation for structural dynamics. *Journal of the Engineering Mechanics Division* 85(3):67-94.

Park JS, Kim JS, Lee JK (2001) Robust control of maglev vehicles with multimagnets using separate control techniques. *KSME International Journal* 15(9):1240-1247, DOI: 10.1007/BF03185664

Popp K, Schiehlen W (1975) Dynamics of magnetically levitated vehicles on flexible guideways. *Vehicle System Dynamics* 4(2-3):195-199, DOI: 10.1080/00423117508968491

Ren S, Romeijn A, Klap K (2010) Dynamic simulation of the maglev vehicle/guideway system. *Journal of Bridge Engineering* 15:269-278, DOI: 10.1061/(ASCE)BE.1943-5592.0000071

Shi J, Wei Q, Zhao Y (2007) Analysis of dynamic response of the high-speed EMS maglev vehicle/guideway coupling system with random irregularity. *Vehicle System Dynamics* 45(12):1077-1095, DOI: 10.1080/00423110601178441

Sinha PK, Pench G, Abbassi HA (1991) Digital control of an electromagnetic suspension system using the TMS-32020 signal processor. *Automatica* 27(6):1051-1054, DOI: 10.1016/0005-1098(91)90142-O

Suzuki S, Kawashima M, Hosoda Y, Tanida T (1984) HSST-03 system.

IEEE Transactions on Magnetics 20(5):1675-1677, DOI: 10.1109/TMAG.1984.1063210

Yang YB, Yau JD, Wu YS (2004) Vehicle–bridge interaction dynamics with applications to high-speed railways. World Scientific, Singapore, 355-357

Yau JD (2009) Vibration control of maglev vehicles traveling over a flexible guideway. *Journal of Sound and Vibration* 321(1-2):184-200, DOI: 10.1016/j.jsv.2008.09.030

Yau JD (2010a) Interaction response of maglev masses moving on a suspended beam shaken by horizontal ground motion. *Journal of Sound and Vibration* 329(2):171-188, DOI: 10.1016/j.jsv.2009.08.038

Yau JD (2010b) Response of a maglev vehicle moving on a series of guideways with differential settlement. *Journal of Sound and Vibration* 324(3-5):816-831, DOI: 10.1016/j.jsv.2009.02.031

Yau JD (2010c) Aerodynamic vibrations of a maglev vehicle running on flexible guideways under oncoming wind actions. *Journal of Sound and Vibration* 329(10):1743-1759, DOI: 10.1016/j.jsv.2009.11.039

Zhang L, Huang JY (2019) Dynamic interaction analysis of the high-speed maglev vehicle/guideway system based on a field measurement and model updating method. *Engineering Structures* 180:1-17, DOI: 10.1016/j.engstruct.2018.11.031

Zhang ZC, Lin JH, Zhang YH, Zhao Y, Howson WP, Williams FW (2010) Non-stationary random vibration analysis for train–bridge systems subjected to horizontal earthquakes. *Engineering Structures* 32(11):3571-3582, DOI: 10.1016/j.engstruct.2010.08.001

Zhao CF, Zhai WM (2002) Maglev vehicle/guideway vertical random response and ride quality. *Vehicle System Dynamics* 38(3):185-210, DOI: 10.1076/vesd.38.3.185.8289

Zheng XJ, Wu JJ, Zhou YH (2005) Effect of spring non-linearity on dynamic stability of a controlled maglev vehicle and its guideway system. *Journal of Sound and Vibration* 279(1-2):201-215, DOI: 10.1016/j.jsv.2003.10.025